Spectral Tuning in Biology II: Structural Color

10

Shuichi Kinoshita, Helen Ghiradella, and Lars Olof Björn

10.1 Introduction

Structural colors are formed by the interaction of light with materials with very specific (and usually complex) micro- and nanoscale architecture; in biological systems, they are likely to occur in stiff, nonliving "biological materials." These nonliving materials include arthropod exoskeleton, bird feathers, fish scales, mollusk shells (particularly their inner linings), and the like.

Structural colors come in several basic types: let us begin here with a discussion of *iridescence*. Iridescence is defined as a category of color that changes with the illuminating and viewing angles; it is abundant in the animal kingdom as brilliant, often metallic, colors characteristic of many birds, fish, insects, marine annelids, and other invertebrates; it has more recently also been described in plants (Glover and Whitney 2010, Lee 2007).

Pioneering work on the subject was done by Mason (1923a, b, 1926, 1927a, b); since then, there has been an explosion of interest in these systems. Recent reviews include Fox (1976), Ghiradella (1991, 1998), Herring (1994, 2002), Parker (1998, 1999, 2000), Srinivasarao (1999), Vukusic and Sambles (2003), Kinoshita and Yoshioka (2005a, b), Kinoshita et al. (2008), Prum (2006), Berthier (2007), and Kinoshita (2008, 2013).

S. Kinoshita (✉)
Graduate School of Frontier Biosciences, Osaka University, Osaka, Japan
e-mail: skino@fbs.osaka-u.ac.jp

H. Ghiradella
Department of Biology, University at Albany, Albany, NY, USA
e-mail: hghff@albany.edu

L.O. Björn
School of Life Science, South China Normal University, Guangzhou, China

Department of Biology, Lund University, Lund, Sweden
e-mail: Lars_Olof.Bjorn@biol.lu.se

Let us start by focusing on a particular iridescent form, the biological mirror. As those readers who have driven on a country road at night know, many night-active wild animals have efficient reflectors in their eyes, as do our favorite pets, dogs and cats. These reflectors, located in the back of the eye behind the retina, double the sensitivity of the eyes to light. They do this by throwing photons that have escaped absorption by the light-sensitive pigments during their first passage through the retina, back through the retina again to give it a second chance to absorb them.

Some light-emitting organs of marine animals have reflectors like those behind the headlights of a car, which throw the light in a certain direction. Many fish scales act as "body mirrors" that reflect the downwelling daylight back towards the water surface, making it easier for their owners to avoid detection. There are even eyes that have mirrors as image-forming optical elements (Land and Nilsson 2002), somewhat analogous to astronomical reflecting telescopes.

These biological mirrors are built up of alternating layers of materials of high and low refractive index, forming a structure we call a "multilayer thin-film stack." We have previously (Chap. 1) treated reflection at a single boundary between media with different refractive indices. When several such boundaries are stacked upon one another, we cannot simply compute the reflectance at each of them using Fresnel's formulas (Section 1.9, in Chap. 1) nor compute the transmittance by taking their product for the following two reasons: (1) there will be multiple reflections of photons bouncing back and forth between the boundaries, and (2) there will be interference effects.

To understand how such complex mirrors function, we have to consider the phases of electromagnetic oscillations, which was not necessary for a single boundary. Phase and phase difference are usually expressed in angular measure (radians), where 2π radians (360°) correspond to a period of the electromagnetic oscillation. Reflection of light traveling from a medium of lower to one of higher refractive index differs in one important respect from reflection of light traveling in the other direction (Fig. 10.1): during reflection towards a

L.O. Björn (ed.), *Photobiology: The Science of Light and Life*,
DOI 10.1007/978-1-4939-1468-5_10,

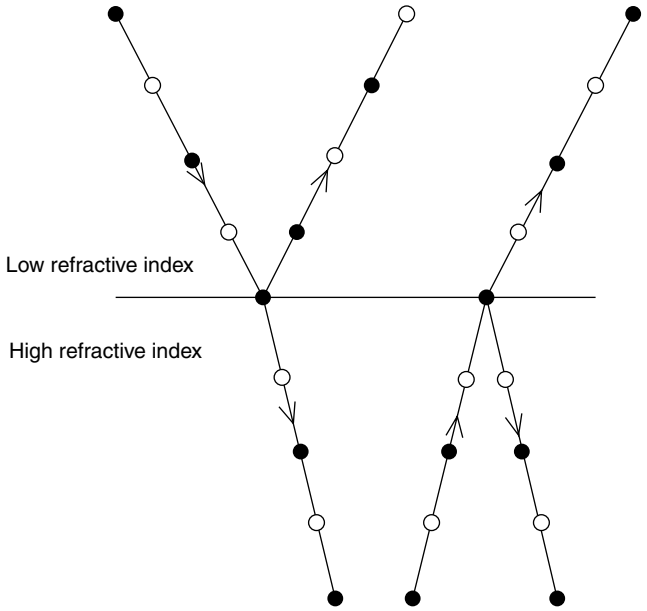

Fig. 10.1 Reflections at an interface between media of higher and lower refractive index. *Filled* and *empty circles* denote opposite phases (i.e., phases differing by π radians) of the electromagnetic waves

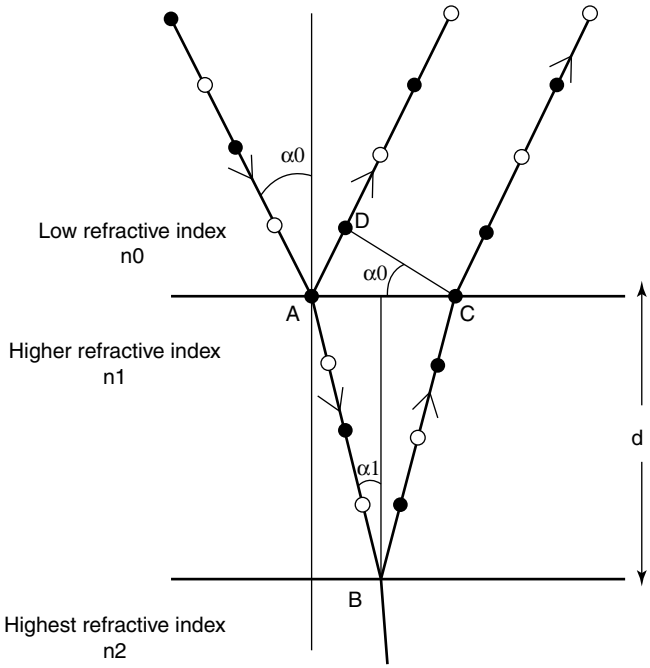

Fig. 10.2 Phase relations during reflection at two consecutive phase boundaries. The drawing is for the case $n_0 < n_1 < n_2$, corresponding to, e.g., the antireflective coating on a camera lens. In this case phase reversal takes place at both reflective surfaces, while with a soap film, the reversal takes place only at the first surface interacting with light

denser medium, the oscillation undergoes a phase change by π radians (180°). The detailed general treatment of reflection in multilayer stacks is complicated. We shall therefore focus here on some special cases, which are more easily understood and nevertheless demonstrate more general principles.

In addition to the multilayer stacks, we will describe some newly developing research, which is related to optical responses due to such completely different structures as regular arrangements of elements, on the one hand, and random ("spongy") structures on the other. The former correspond to so-called photonic crystals, whose study has been advanced in a surprisingly quick manner after the concept was established in the 1980s. However, in natural worlds, photonic crystals are found to be very common, appearing as the play of color in opal, brilliant wings in birds, and iridescent wings of butterflies and beetles, to name a few.

The spongy structural mode is related to a phenomenon called Tyndall blue or Rayleigh scattering and has long been believed to be the origin of non-iridescent blue colors of dragonflies and kingfishers. However, recent investigations have shown that even these colors are not due to simple light scattering processes, but are also related to the interference effect.

10.2 Reflection in a Single Thin Layer

Everyone is familiar with the reflections from soap films and knows that a range of colors can be produced by such reflection. In this case, we have a thin film of higher refractive index (approximately that of water) with the same medium (air) on both sides of the film. We can generalize this by considering a bulk medium of one refractive index, n_0, on one side, a thin film with a different refractive index, n_1, and on the other side a bulk medium with the third refractive index, n_2 (Fig. 10.2). We refer to these three media as being of orders 0, 1, and 2, respectively. For the soap film case, the relation between these indices is given as $n_0 = n_2 < n_1$. (A well-known example in which the relation $n_0 < n_1 < n_2$ holds is the antireflective coating on a camera lens.) As we shall see later, we can treat these and similar cases with the same set of equations.

We denote the incidence angle by α_0 and the angle of refraction in the film as α_1; Snell's law then gives the relationship $n_0 \sin\alpha_0 = n_1 \sin\alpha_1$, or $\sin\alpha_1 = n_0 \sin\alpha_0 / n_1$.

The ordinary Fresnel reflection factors for a single surface between bulk media 0 and 1 (Chap. 1) are given as

$$R_{01}^{p} = \left[\frac{n_1 \cos\alpha_0 - n_0 \cos\alpha_1}{n_1 \cos\alpha_0 + n_0 \cos\alpha_1} \right]^2,$$

$$R_{01}^{s} = \left[\frac{n_0 \cos\alpha_0 - n_1 \cos\alpha_1}{n_0 \cos\alpha_0 + n_1 \cos\alpha_1} \right]^2,$$

for light having the electric vector parallel to the plane of incidence (p-polarization) and perpendicular to it

(*s*-polarization), respectively. These give the reflection coefficients for power or intensity, and of course they are always represented by positive real numbers.

It turns out that for a thin film, due to the interference effect, not only these angle-dependent factors, but also another angle-dependent factor, has to be taken into account. This is a function also of the layer thickness (d), the vacuum wavelength (λ), and the refraction index (n_1) of the film. To compute this, we first calculate the phase difference between the rays reflected from the first and from the second surface (Fig. 10.2). This phase difference can be thought of as composed of four components. The first is due to the phase reversal at the first surface. The phase difference is π radians for $n_1 > n_0$, as with the soap film and the camera lens, but it is 0 for $n_1 < n_0$. The second is due to the longer distance (AB + BC) traveled inside the film with the refraction index of n_1 by the ray reflected from the second surface. Therefore, the phase difference results in $2n_1 d(2\pi/\lambda)/\cos\ \alpha_1$ radians. The factor 2 at the front stems from the fact that the ray reflected from the second surface traverses the film twice, and $n_1 d$ is the "optical thickness" of the film, i.e., the geometrical thickness corrected for the shortening of the wavelength of light in proportion to the refraction index.

The third component of the phase difference is due to possible phase reversal during reflection at the second surface. It is 0 in the soap film case, because $n_1 > n_2$, and π radians in the camera lens case, because $n_1 < n_2$.

The fourth component of the phase difference is due to the shorter distance, AD, in Fig. 10.2, traveled in the n_0 medium. This phase difference is calculated as

$$\begin{aligned}
&\mathrm{AD}\cdot n_0(2\pi/\lambda) = \mathrm{AC}\cdot\sin\ \alpha_0 \cdot n_0(2\pi/\lambda)\\
&\quad = 2d\tan\ \alpha_1 \cdot \sin\ \alpha_0 \cdot n_0(2\pi/\lambda)\\
&= 2d\left(\sin\ \alpha_1/\cos\ \alpha_1\right)\cdot n_1 \sin\ \alpha_1(2\pi/\lambda)\\
&= 2n_1 d\sin^2\alpha_1(2\pi/\lambda)/\cos\ \alpha_1\ (\text{radians}).
\end{aligned}$$

If we calculate the phase differences between these two pathways, we obtain

$$\begin{aligned}
&2n_1 d(2\pi/\lambda)/\cos\ \alpha_1 - 2n_1 d\sin^2\alpha_1(2\pi/\lambda)/\cos\ \alpha_1\\
&\quad = 2n_1 d\left(1-\sin^2\alpha_1\right)(2\pi/\lambda)/\cos\ \alpha_1\\
&\quad = 2n_1 d\cos^2\ \alpha_1(2\pi/\lambda)/\cos\ \alpha_1\\
&\quad = 2n_1 d\ \cos\ \alpha_1(2\pi/\lambda)(\text{radians}),
\end{aligned}$$

which directly corresponds to the total phase difference in the case of $n_0 < n_1 < n_2$, because the phase reversal at each surface is canceled, while in case of $n_0 = n_2 < n_1$, we have to add π to the above formula, corresponding to the phase reversal at the first surface.

The Fresnel formulas given above, with expressions in squared brackets, represent intensity reflection coefficients. For many computations, however, it is advantageous to work with the corresponding unsquared expressions, so-called amplitude reflection coefficients, describing the change in amplitude of the electric wave upon reflection (the energy of the wave is proportional to the square of the amplitude). These coefficients, in contrast to the intensity reflection coefficients, can be either positive or negative (if light-absorbing materials are involved, the amplitude reflection coefficient is represented by a complex number, but we shall not consider this case here). A negative amplitude reflection coefficient means that the electric field changes direction during reflection, in other words, that we have a phase change of π radians. Therefore, when we do calculations based on the amplitude reflection coefficients, we do not have to worry about the phase changes of π radians during reflection, since they will come automatically with the sign of the amplitude reflection coefficient used.

The following QuickBasic program will compute the reflectance over a wavelength range of 0.3–1 μm for a thin film with refractive index n_1 between media with refractive indices n_0 (incidence side) and n_2 (output side), respectively. In reality, the multiple reflection within the film generally takes place and effectively influences the reflection intensity when the refractive index of the film is much higher or the output side is replaced by a metallic substance. However, we neglect this effect and take only the first and second reflections into account. Furthermore, the refractive indices will generally vary with wavelength, but this has also not been taken into account. Thus, the reflectance of the single thin layer is expressed as

$$R^{s,p} = \left(r_{01}^{s,p}\right)^2 + \left(r_{12}^{s,p}\right)^2 + 2r_{01}^{s,p} r_{12}^{s,p}\cos\ \delta,$$

where $r_{01}^{s,p}$ and $r_{12}^{s,p}$ are the Fresnel amplitude reflection coefficients corresponding to *s*- and *p*-polarizations for the interface between the bulk medium 0 and the film 1 and those between the film 1 and the bulk medium 2, respectively. δ is the phase difference described above and is expressed as $\delta = 2n_1 d\cos\ \alpha_1(2\pi/\lambda)$. If we run on a Macintosh computer, the result will appear in the clipboard and can be transferred to other programs from there. If you wish to have the output in another form, line 200 should be modified accordingly, and for other computers and Basic dialects, modifications may have to be made.

```
INPUT "incidence angle in degrees =",
a0:pi = 3.14159: a0 = a0 * pi/180
INPUT "thickness of thin layer in micrometres =", d
```

```
INPUT "refractive index of medium 0=", n0
INPUT "refractive index of thin layer=", n1
INPUT "refractive index of medium 1=", n2
sina1 = n0 * SIN(a0)/n1: a1 = ATN(sina1/SQR(1-sina1 * sina1))
sina2 = n1 * sina1/n2: a2 = ATN(sina2/SQR(1-sina2 * sina2))
50 :PRINT "Enter p for parallel (p) polarization, s for perpendicular (s) polarization."
PRINT "Polarization directions are of electric vector relative to incidence plane."
INPUT "electric vector direction", polarization$
IF polarization$ = "p" THEN 150
IF polarization$ = "s" THEN 100
PRINT "Mistake! Try again!": GOTO 50
100 : r1 = (n0 * COS(a0)-n1 * COS(a1))/(n0 * COS(a0)+n1 * COS(a1))
r2 = (n1 * COS(a1)-n2 * COS(a2))/(n1 * COS(a1)+n2 * COS(a2)):GOTO 170
150 :r1 = (n1 * COS(a0)-n0 * COS(a1))/(n0 * COS(a1)+n1 * COS(a0))
r2 = (n2 * COS(a1)-n1 * COS(a2))/(n1 * COS(a2)+n2 * COS(a1)):GOTO 170
170 :OPEN "O",1,"clip:"
FOR L = .3 TO 1 STEP .01
delta=4*pi * n1 * d/L*COS(a1)
I = (r1 * r1+r2 * r2+2 * r1 * r2 * COS(delta))
I = I/(1+r1 * r1 * r2 * r2+2 * r1 * r2 * COS(delta))
200: PRINT#1, I: NEXT L: CLOSE 1: END
```

We show in Fig. 10.3 the output of this program for a soap film ($n_1=1.33$) of 0.33-μm thickness with $n_0=n_2=1$, both for normal incidence ($\alpha_0=0$) and for 45° incidence angle; in the latter case for both polarizations. This film would look yellow in a perpendicular direction and bluish green in a 45° direction. Note that the reflection spectrum shifts to a shorter wavelength with increasing incidence angle, that there are in each spectrum several peaks corresponding to phase shifts of integer multiples of 2π, and that for oblique angles, the *s*-polarized light is reflected better than the *p*-polarized light.

The wavelengths giving the maximum and minimum reflectance are easily obtained according to the value of $\cos\delta$ and the sign of the product $r_{01}^{s,p}\, r_{12}^{s,p}$ in the above formula. In the case of $n_0=n_2<n_1$, for example, the conditions for the maximum and minimum reflectance are given as $\cos\delta=-1$

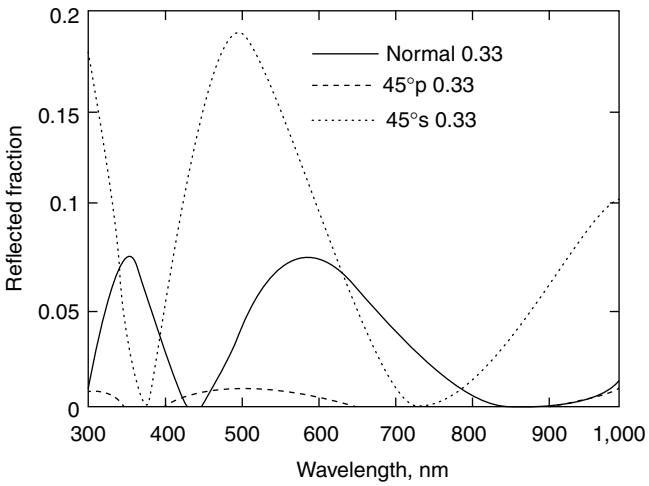

Fig. 10.3 Reflection in a soap film of 0.33-μm thickness and the refractive index of 1.33

and $\cos\delta=1$, because the sign of the product becomes negative, which result in $2n_1 d\cos\alpha_1(2\pi/\lambda)=(2m-1)\pi$ and $2n_1 d\cos\alpha_1(2\pi/\lambda)=2m\pi$, respectively. Thus, we obtain

$$\lambda_{\max}=\{4n_1 d/(2m-1)\}\cos\alpha_1=\{4n_1 d/(2m-1)\}\sqrt{1-(n_0/n_1)^2\sin^2\alpha_0},$$

$$\lambda_{\min}=\{4n_1 d/(2m)\}\cos\alpha_1=\{4n_1 d/(2m)\}\sqrt{1-(n_0/n_1)^2\sin^2\alpha_0},$$

where m denotes any positive integer and we have used the relation $\cos\alpha_1=\sqrt{1-(n_0/n_1)^2\sin^2\alpha_0}$.

Next we run the program for a typical camera lens antireflective coating with $n_0=1$, $n_1=1.38$ (corresponding to magnesium fluoride), and $n_2=1.89$ (heaviest flint glass). The optical thickness (thickness × refractive index) of the layer is adjusted to correspond to one quarter wavelength of yellow light (589 nm) in the layer, i.e., (0.589/4)/1.38 μm (Fig. 10.4). The wavelengths giving the maximum and minimum reflectance in this case are obtained by interchanging $\lambda_{\max}$ and $\lambda_{\min}$ in the above relations.

To obtain zero reflection with an antireflective coating on a lens, two conditions must be fulfilled: (1) the optical thickness of the coating film must be equal to one quarter of the wavelength of light (or this plus an integer multiple of the wavelength), which can be achieved only for a certain wavelength; and (2) the coating material must have a refraction index which is the square root of the product of the refractive indices of the outer medium (air) and the lens material (i.e., $n_1=\sqrt{n_0 n_2}$). In practice, compromises have to be made.

The reader might wonder what the construction of antireflective coating on a camera lens has to do with photobiology. The fact is that even some eyes, notably in the insect orders Lepidoptera and Diptera, have antireflective surfaces (Bernhard et al. 1965, 1968, 1970; Parker 1999, 2000; Yoshida

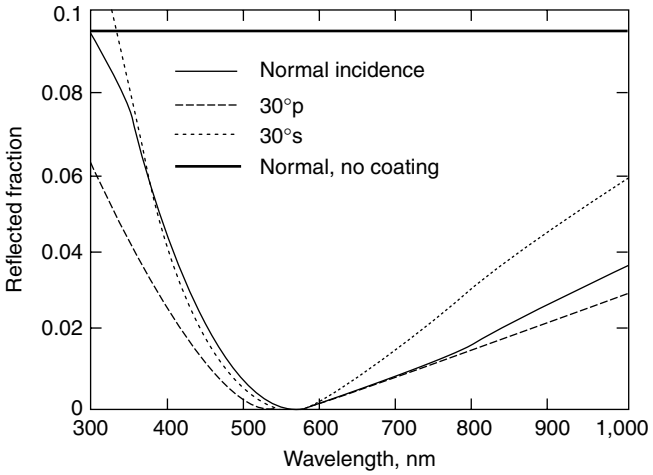

Fig. 10.4 Reflectance of a lens of heaviest flint glass ($n_1 = 1.89$) coated with a quarter-wave thickness (0.107 μm) of magnesium fluoride (MgF2, $n_1 = 1.38$). Reflected fraction of the incident light is shown for normal incidence and for 30° incidence angle with different polarizations. For comparison, the reflected ratio at normal incidence without coating is also shown. For oblique angles, even higher reflectance would be obtained without coating. The mixture of violet-blue and red reflected light gives such a lens a purple tint

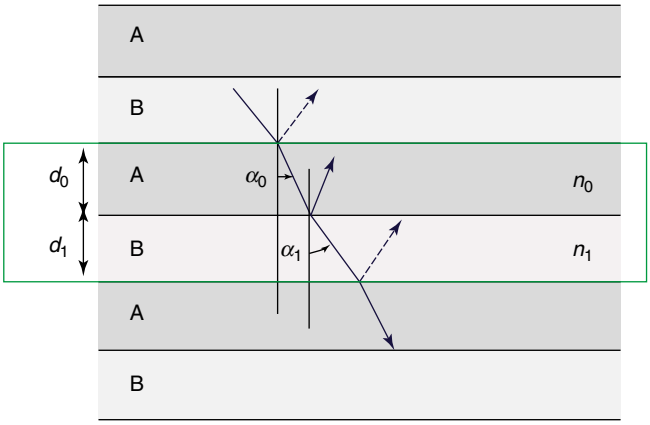

Fig. 10.5 Schematic illustration of multilayer stack. The dashed arrows indicate the phase reversal taking place during reflection. Complete constructive interference is obtained when the sum of (**A**) and (**B**) stacks is regarded as a film satisfying the thin-film interference condition for antireflective coating, while a single (**A**) or (B) layer satisfies the soap-bubble condition

et al. 1996; Yoshida 2002; Stavenga et al. 2006a). In this case, however, the antireflective surface is not obtained by addition of a layer of material of a different refractive index, but by finishing off the bulk material with tapering "nipples" smaller than the wavelength of the light, which effectively provide a gradual change in refractive index from that of the bulk material to that of air. The main biological advantage of the antireflective surface might be to make the bearer of the eyes less conspicuous by avoiding a shiny surface ("eyeshine") (Stavenga et al. 2006) and to some extent to improve vision.

This type of antireflective surface, usually called "moth-eye structure," has become one of the most advanced achievements of recently developing nanotechnology and has often been employed to reduce reflective loss at the surfaces of solar cells. The advantage of this "biological-inspired" antireflective coating lies in its extraordinarily wide angular and wavelength ranges, which cannot be achieved by simple film-type antireflective coatings, even when two or more layers are employed. (It is also an example of "biomimicry," an increasingly important technological approach to design, to which we will briefly return towards the end of this chapter.)

10.3 Reflection by Multilayer Stacks

We shall now come to a more complicated case of multilayer stacks forming efficient biological mirrors with nearly 100 % reflectance. The most important case is that of normal incidence. Eyes, for instance, are constructed such that light hits the retina, and therefore also the reflective backing of the retina, almost perpendicularly. However, using the computer program shown later, oblique incidence and both *s*- and *p*-polarizations can be handled.

Interference phenomena due to periodic multilayer stacks are qualitatively understood in terms of periodic piling of a pair of thin layers. Consider two layers designated as A and B with thickness d_0 and d_1 and refractive indices n_0 and n_1, respectively, as illustrated in Fig. 10.5. We will tentatively assume $n_0 > n_1$. If we consider a certain pair of AB layers, the phases of the reflected light at the upper and lower B-A interfaces both change by π radians, because the condition $n_0 > n_1$ holds. Thus, the relation similar to the antireflective coating described in the previous section is applicable. Taking into account that the present system consists of two layers, the wavelength of maximum reflectance will be given as

$$\lambda_{\max} = 2\{n_0 d_0 \cos \alpha_0 + n_1 d_1 \cos \alpha_1\}/m,$$

with the angles of refraction in the A and B layers as α_0 and α_1, respectively.

Furthermore, if we consider only the A layer within the AB layer, the phase of the reflected light does not change at the A-B interface, while it does change at the B-A interface. Thus, an interference condition corresponding to the soap film case can be applied:

$$\lambda_{\max} = 4n_0 d_0 \cos \alpha_0 / (2m' - 1),$$

where m' is a positive integer satisfying the condition $m' \leq m$. If the above two conditions are simultaneously satisfied at the same wavelength, the reflected light from the A-B interfaces adds to that from the B-A interfaces so that the multilayer will give the maximum reflectance. In particular,

the condition $m = 1$ and $m' = 1$ corresponds to the lowest-order reflection with the optical thicknesses of the A and B layers equal to each other. Land called this case "ideal stack" or "ideal multilayer" (Land 1972).

On the other hand, if the thicknesses of the A layers do not satisfy the latter relation, while the sum of the A and B layers satisfies the former one, the reflection at the A-B interface works more or less destructively so that the peak reflectance will decrease. This case is called a "non-ideal stack." An ideal stack is effective to increase the reflectance, whereas its reflection band width is also increased considerably. On the other hand, a non-ideal reflection band width can be suppressed, which is often effective to show the color more clearly.

The following computer program is based on the treatise by Huxley (1968) and is in agreement with the example treated by Land (1966).

```
pi = 3.14159
INPUT "refraction index of medium and spaces", na
INPUT "thickness of spaces, micrometres", da
INPUT "number of plates = ", p
INPUT "thickness of plates, micrometres", db
INPUT "refraction index of plates", nb
INPUT "incidence angle, degrees", aa:IF aa = 0 THEN aa = .001:aa = pi * aa/180
sinab = na * SIN(aa)/nb:ab = ATN(sinab/SQR(1-sinab * sinab))
27 : INPUT "choose polarization, p for parallel, s for perpendicular", pol$
IF pol$ = "s" THEN 29
IF pol$ = "p" THEN 30
PRINT "MISTAKE! Try again!"
28 : GOTO 27
29 :r = SIN(aa-ab)/SIN(aa+ab):GOTO 31
30 : r = -TAN(aa-ab)/TAN(aa+ab)
31 :OPEN "O",1,"clip:"
FOR L = .4 TO .85 STEP .001
fia = (2 * pi/L) * da * na * COS(aa):fib = (2 * pi/L) * db * nb * SQR(1-sinab * sinab)
kprim = -(COS(fia+fib)-r * r * COS(fia-fib))/(1-r * r)
k = (SIN(fia+fib)-r * r * SIN(fia-fib))/r/SIN(fib)/2
IF kprim * kprim<1 GOTO 100
REM In the following case mu is real
mu1 = kprim+SQR(kprim * kprim-1)
mu2 = kprim-SQR(kprim * kprim-1)
90 :murat = mu1/mu2:IF murat>1 THEN murat = 1/murat
```

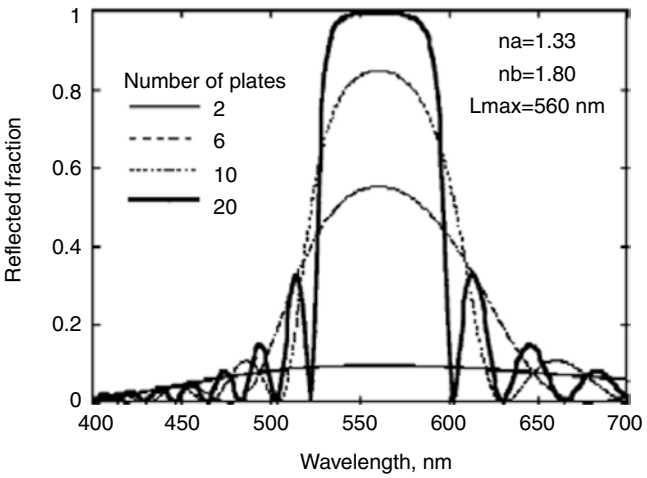

Fig. 10.6 Reflectance at normal incidence of a stack of guanine plates ($n = 1.80$) with spaces between the plates having a refractive index like that of seawater ($n = 1.34$). The thickness of plates and of spaces was chosen such that thickness times refractive index (optical path length) amounts to 140 nm. This leads to high reflection at 4 × 140 nm = 560 nm

```
95 :m2 = (murat)^ p
RR= 1/(1+4 * m2 * (1-k * k)/(1-m2)/(1-m2)):GOTO 200
100 :REM In the following case mu is complex
costheta = (COS(fia+fib)-r * r * COS(fia-fib))/(1-r * r)
theta = ATN(SQR(1-costheta * costheta)/costheta)
RR= 1/(1+(k * k-1)/SIN(p * theta)/SIN(p * theta))
200 :PSET(1000 * (L-.39),310-300 * RR):PRINT# 1,RR
300 :NEXT L:CLOSE 1
400 :FOR L = .4 TO .85 STEP .05
CALL MOVETO(1000 * (L-.39),310):CALL LINETO(1000 * (L-.39),320)
IF 10 * L<>INT(10 * L) THEN 500
CALL MOVETO(1000 * (L-.41),330): PRINT 1000 * L;"nm"
500 :NEXT L
END
```

Figure 10.6 shows examples of the output of this computer program. Within a certain wavelength range, about 100 nm, the reflectance reaches nearly 100 % for only 20 high index layers, i.e., 40 interfaces, while it is lower outside this region and oscillates with wavelength; the number of these oscillations increases with an increasing number of layers. In reality this results in shiny reflectance only within a certain wavelength range, which gives a colored appearance to the surface, as can be seen in, for instance, green and blue beetles.

Although Huxley's method of calculating the reflectance has the advantage of giving physical insight into such spectral features as the reflection band width and the oscillatory structures, it has an essential difficulty in freely changing such parameters as thicknesses and refractive indices of the layers. For this purpose, a transfer matrix (Born and Wolf 1959; Kinoshita 2013) and iterative methods (Kinoshita 2008) are often employed, which are applicable to multilayer stacks of any kind, even when the repetitive structure is absent and the refractive indices of the incidence and output media are different.

The hue of the metallic shine due to a multilayer stack also shows a typical iridescent nature: the color changes with incidence and/or viewing angles (Fig. 10.7; see also Fig. 10.4). Common examples where this effect can be seen in Europe are the heads of male mallards, which change between green and blue depending on from where they are seen. However, the angle-dependent color changes do not result only from the multilayer construction; there are also many examples where gratings (Chap. 3) produce the colorful effects (Pfaff and Reynders 1999; Srinivasarao 1999). Some of these latter include plants: for example, Glover and Whitney (2010) report that in several species of plants, epidermal cells are elongated and flat, with ridged cuticle that acts as a diffraction grating. In these cases, the iridescence often seems to be in the UV. In the rock dove, the color of the neck feather changes between green and purple, which is due to a single thin-layer mechanism at the outer cortex of the barbule (Yoshioka et al. 2007).

The structural color of the jewel beetle, *Chrysochroa fulguidissima*, is an excellent example of spectral tuning due to a multilayer stack. As shown in Fig. 10.8a, its elytra show shiny metallic green with copper-brown stripes on them. The peaks of the reflection spectra for green and copper-brown regions of the elytra were reported to be 550 nm and 750–950 nm, respectively (Hariyama et al. 2005). The electron microscopic observation showed that the epicuticle located just below the elytron surface was covered with several alternate layers of electron-dense and electron-lucent regions as shown in Fig. 10.8b. The reflection spectrum calculated using the wavelength-dependent refractive indices determined recently was actually in good agreement with that of the experiment (Yoshioka and Kinoshita 2011).

A tropical fish, the neon tetra, gives another interesting example. The *iridophores*, pigment cells containing multilayer stacks of guanine crystal plates, located under a blue stripe of a neon tetra have been extensively investigated since the 1970s (Lythgoe and Shand 1982; Nagaishi and Oshima 1992). It has been shown that a pair of stacks is present within each iridophore and in each stack are included many hexagonally shaped guanine platelets (see Fig. 10.9), which are enclosed by membranes and arranged regularly with a

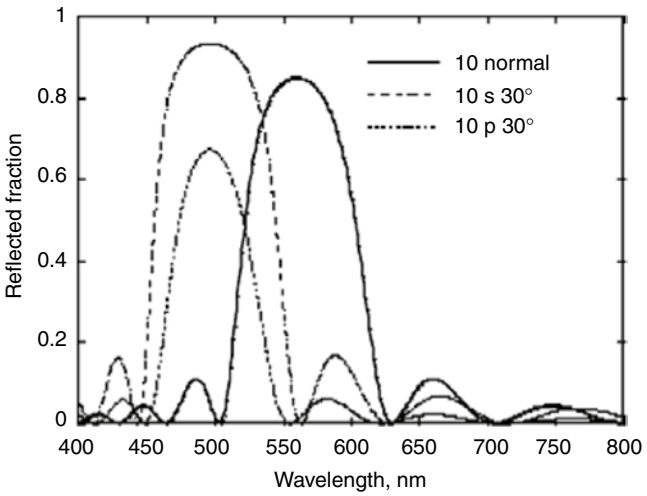

Fig. 10.7 Reflectance of a stack of 10 plates similar to those in Fig. 10.5 and with the same medium in between. Reflectance was computed for normal incidence and for an incidence angle of 30° and both polarizations

constant inclination angle to the surface. The inclination of the platelets may be effective to reflect light in a horizontal direction when illuminated from a dorsal direction. Thus, the color of the stripe is a typical case of multilayer interference.

The noteworthy point in this system is that its color changes from violet (under dark conditions) to yellow (under bright illumination) with the ambient light and also with the physiological conditions. Two major mechanisms have been proposed for this change: one is a change in the spacing between the platelets (Lythgoe and Shand 1982) and the other is a change in their inclination angle (Nagaishi and Oshima 1992) (see Fig. 10.9c). Recent experimentation has proved that the latter mechanism, called the "Venetian blind model," is more suitable to explain the experimental results (Yoshioka et al. 2011).

There exist other cases of "tunable" reflectors in the natural world. Hinton and Jarman (1972, 1973) describe beetles that can change color quickly by shifting between air and liquid in the cuticle; something similar is reported in the Panamanian tortoise beetle (Vigneron et al. 2007). Here there are within the elytra and elsewhere "chirped" layers of cuticle (see below) that have within them porous patches that can reversibly hold fluid. When the system is hydrated, it reflects a multilayer-based gold color, but when dehydrated, it becomes translucent and reveals an underlying red (non-structural) color. In other words, the system is reversibly deploying an iridescent screen.

A different mechanism, and one that is an exception to the rule of "nonliving materials" providing biological iridescent colors, is reported in the color-bearing iridocyte cells of certain squids (DeMartini et al. 2013). These cells have at their

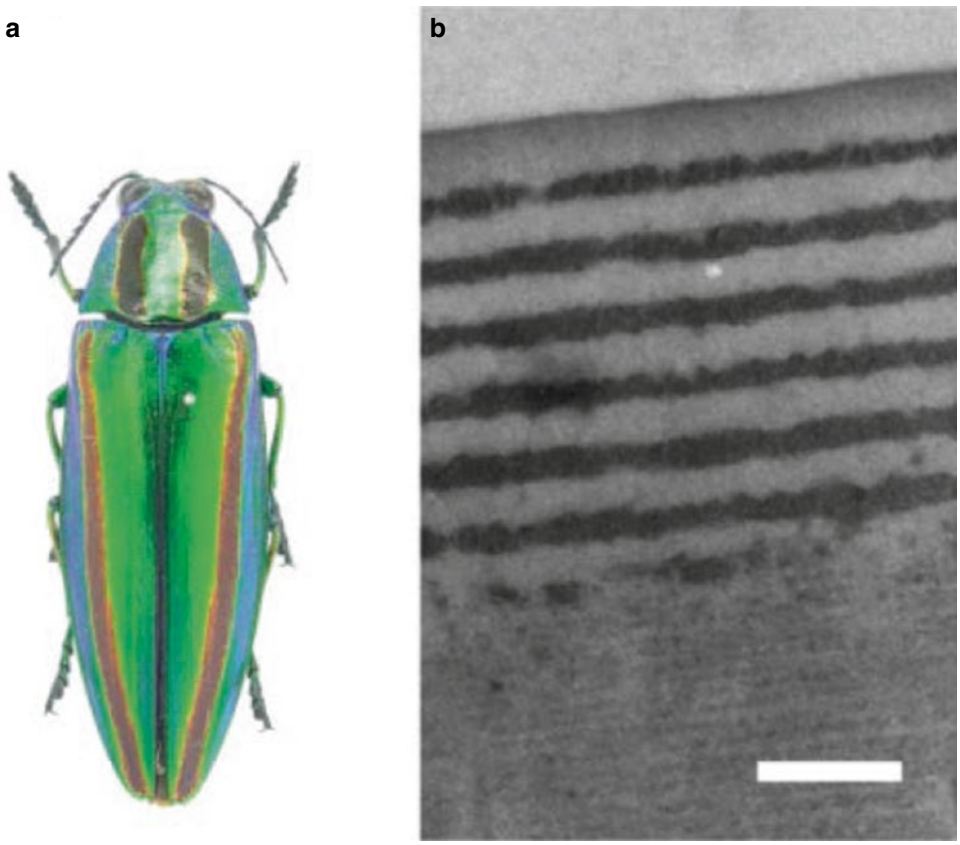

Fig. 10.8 (**a**) Jewel beetle, *Chrysochroa fulgidissima*, and (**b**) an electron micrograph of the multilayer system located beneath the elytron surface [the copper-brown striped part in (**a**)]. Scale bar: 500 nm (Reproduced from Yoshioka and Kinoshita 2011)

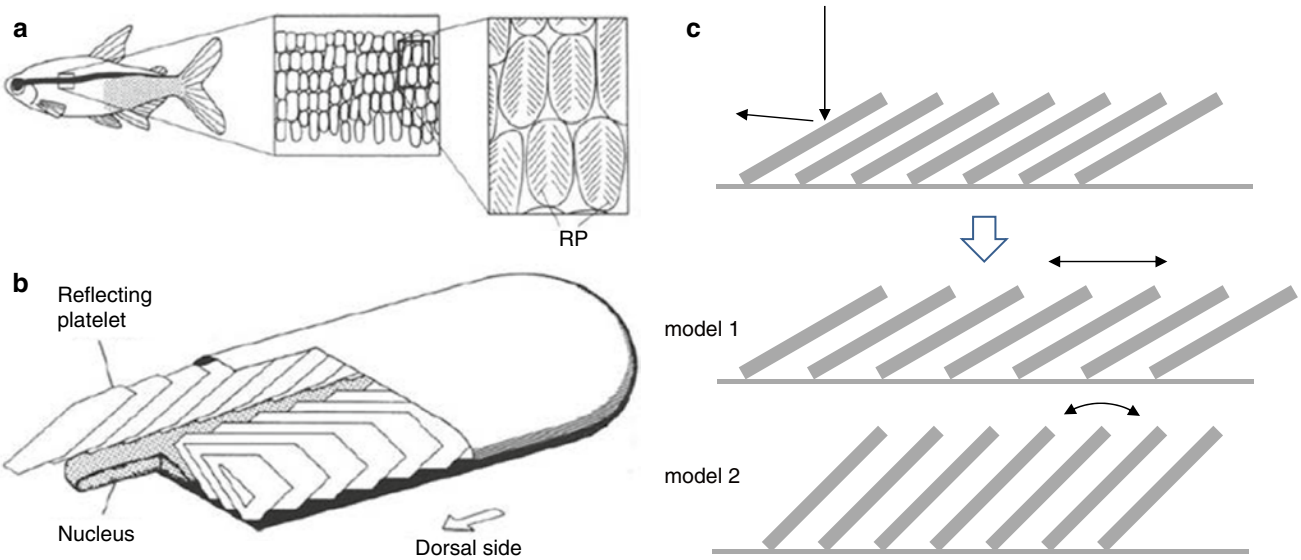

Fig. 10.9 Schematic illustrations of (**a**) a neon tetra and (**b**) its iridophore, which contains mainly two stacks of the thin light-reflecting platelets (RPs) (Reproduced from Nagaishi and Oshima (1992), with permission). (**c**) Two models for the color change due to the reflecting platelets are explained: model 1 represents the change of the spacing between platelets and model 2 that of the inclination angles

surfaces deep grooves that contain extracellular channels separating fingerlike cellular lamellae. By a reversible chemical cascade involving phosphorylation and condensing of reflecting proteins, the system can change lamella size and hence color from transparent through a spectrum from red to blue, or back again.

In those cases where high reflectance takes place over a wider wavelength range, such as often from the tapeta of eyes, this can be achieved in a number of ways. One mirror with high reflectance in one wavelength band (i.e., with one spacing and thickness of high index plates) can be positioned behind another with a different spectral tuning. Or the dimensions of the layers can be continuously varied from wide to narrow ("chirped layers") or have "chaotically" varying dimensions. An example of an animal in which layer thickness is varied in a way referred to as "doubly chirped" (thickest layers in the center) is the silverfish (Large et al. 2001). In the herring, neutral, silvery reflectance is obtained by a combination of different body surface scales reflecting red, green, and blue wavebands (Denton and Land 1971).

Chemical compounds employed for the layers of high and low refractive indices have a wide variety, depending on the organisms involved. For example, the combination of guanine and aqueous solution is generally used in animal eyes and also in skins of fish, lizards, and frogs; similarly, melanin and cuticle are used in beetle wings, cuticle and air in butterfly wings, and cellulose and aqueous solution in plants.

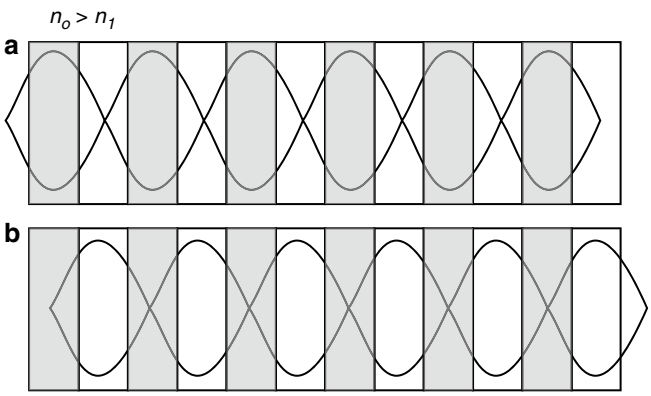

Fig. 10.10 Schematic illustration to explain the origin of the band gap. The light waves propagating to the right and left directions interfere with each other to form a standing wave. Consider a case where the wavelength of the light is twice the periodicity of the structure. (**a**) If the antinode of the standing wave is coincident with the high refractive index layer (n_0), the electromagnetic energy will be the highest, while (**b**) if it is coincident with the low refractive index layer (n_1), the energy will be the lowest; these together give the highest and lowest energy limits of the photonic band gap

10.4 Reflection Based on Photonic Crystals

We have been reviewing so far structural colors as more or less traditionally described, single thin-film or multilayer stacks, but in the 1980s, there appeared in the literature a new phrase, "photonic crystal," to describe many of the materials displaying structural color effects. As this concept was developed, these photonic crystal materials were classified as one, two, or three dimensional (1D, 2D or 3D); the multilayer thin-film stacks qualify as 1D photonic crystals, and despite the complexity of our optical treatment above, these are considered the optically simplest ones.

2D and 3D photonic crystals selectively reflect light within certain wavelength ranges ("photonic band gap") while transmitting others. Where one to punch a regular array of minute holes in a film, one would have a 2D photonic crystal. Biological examples of such iridescent 2D photonic crystals are found in marine polychaetes (Parker et al. 2001), barbules of bird feathers (Prum 2006), hairs of the comb rows of certain ctenophores (Welch et al. 2005), and butterfly scales (Vukusic and Hooper 2005). The ctenophores are especially interesting in that the comb bases rest above the light organs of the animals, and the hairs are apparently simultaneously producing reflected color from incident light and transmitting the bioluminescence from the light organs out into the environment.

3D photonic crystals abound in nature. The mineral opal consists of silica spheres that pack into a 3D face-centered cubic (fcc) lattice; their band gap structure produces their iridescent colors. Analogous structures show up in insect scales, notably in those of certain butterflies (Morris 1975; Ghiradella 1984a, 1985, 1989, 1998) and beetles (Ghiradella 1984b, 1998; Parker et al. 2003).

The origin of the photonic band gap is qualitatively explained, most simply by using a 1D photonic crystal as follows: when a light wave propagates within an alternately layered structure with different refractive indices, the light wave will be partially reflected and partially transmitted at the interfaces between these layers. The light waves thus generated will propagate to the right and left directions in Fig. 10.10 and will interfere with each other to form a standing wave. We consider a case where the wavelength of a light wave within the layers is equal to twice the period of the layers. If the antinode of the standing wave thus created coincides with a high refractive index part, the energy of electromagnetic wave will be the highest, while in the opposite case, it will be the lowest. Thus, for a single wavelength, at least two defining energy values, corresponding to the edge energies of the photonic band gap, will be realized.

When the thickness of one layer becomes narrower than that of the other, the overlap of the standing wave with the layered structure will be incomplete, so that the energy separation and hence the band gap width will be smaller. It is also expected that if the difference of the refractive indices becomes small, the band gap width will be smaller as well. Thus, a sufficient band gap for a visible effect is produced only when the refractive index contrast is large enough and the optical thicknesses of these two layer types are comparable.

The above idea can be used to qualitatively predict the presence of the photonic band gap in 2D and 3D photonic crystals. Consider a case where filled circles are located at

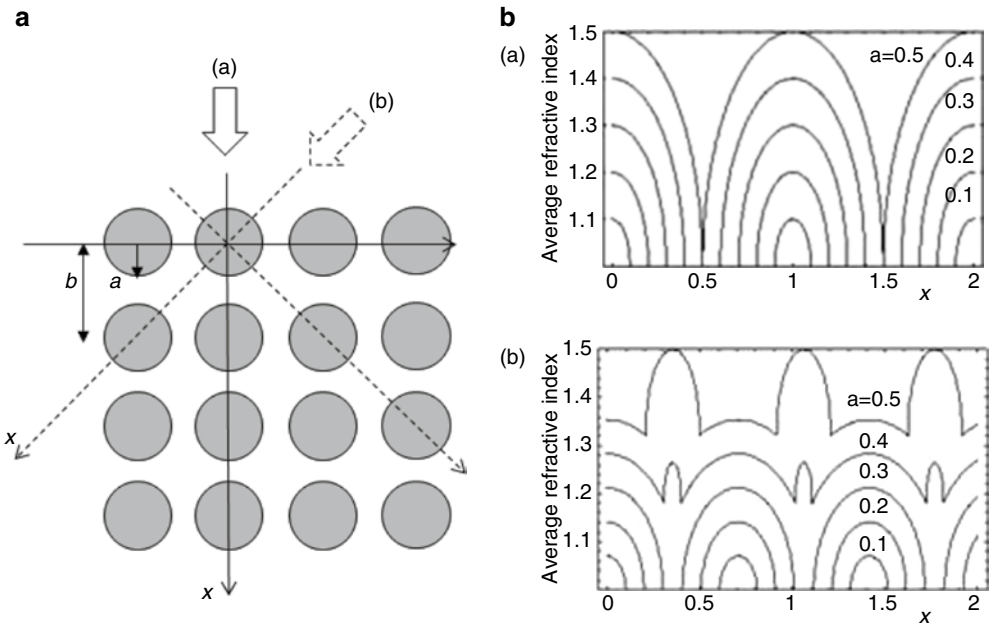

Fig. 10.11 Schematic illustration of a 2D photonic crystal in a square lattice. The average refractive indices are calculated when light is incident (**a**) normal and (**b**) obliquely to the lattice for $a = 0.1 \sim 0.5$, while a lattice constant b is kept constant at unity. The refractive index of the filled circle is set at 1.5, while that of the surrounding medium at 1.0

square lattice points as shown in Fig. 10.11a. When light is incident on the surface of this 2D photonic crystal from direction (a) or (b), the light wave experiences spatial variation of the refractive index during its propagation. The spatial average of the refractive index along the direction perpendicular to the propagation direction is easily calculated as shown in Figs. 10.11b (a) and (b), where the light is assumed to be incident (a) normally and (b) obliquely into the crystal lattice (here, we do not take the refraction at the surface of the photonic crystal into account). It is clear that the refractive index variation is distinct in case (a), particularly when $a = 0.3 \sim 0.5$, where a is the radius of the circle with the lattice constant b set at unity. In contrast, the variation is small in every radius for case (b). Thus, when the radius of the circle is sufficiently large, the refractive index contrast is strongly dependent on the direction of the light propagation. In fact, the band calculation for the refractive index of filled circles of $n = 1.5$, with n of the medium set at 1.0, shows that the photonic band gaps are open only in case (a) and not in case (b).

The band gap characteristics of 2D and 3D photonic crystals are of current interest to the communications industry, which seeks to develop hollow-core versions for more effective optical transmission fibers (another example of *biomimicry*). In such designs, the crystal cladding controls light leakage, while the air-filled core ($n = 1$) will transmit light faster than is now possible with glass fibers. Iridescent hollow-core photonic fibers are known from such biological systems as butterflies (Ghiradella 1994, 1998) and the sea mouse, *Aphrodite*, (Parker et al. (2001), among others.

We will first consider the barbules of the peacock, one of the most well-known avian species displaying structural colors. The colors of peacock feathers have attracted a great deal of scientific attention for more than 300 years and are now known as typical examples of biological photonic crystals. Since the early observations by Hooke (1665) and Newton (1704), it was in the twentieth century that more detailed observation was carried out by Mason (1923b) and then by Durrer (1962).

As shown in Fig. 10.12a, a feather barbule of peacock is somewhat curved along its long axis and slightly twisted from the root. Each barbule has the shape of connected segments of a typical size of 20–30 μm, the surfaces of which are smoothly curved like a saddle (Fig. 10.12b). The sophisticated color-producing structure in the peacock's feather (Fig. 10.12c) was first observed by Durrer (1962) using an electron microscope. It was found that below a cortex surface layer, a total of 3–11 layers of melanin rods (0.11–0.13 μm in diameter and ~0.7 μm in length) were arranged to form a 2D quasi-square lattice (Fig. 10.12c, d) (Zi et al. 2003). At the center of each lattice, a small air hole was present with increasing size towards the lower layers as shown in Fig. 10.12e. The medullary region of the barbule was filled with keratin with a small number of randomly distributed melanin rods and air holes. Durrer found that the rod-to-rod distance perpendicular to the surface correlated with the apparent color of a feather, while that parallel to the surface did not show such a correlation.

Natural photonic crystals are found in a more complete form in butterfly wings. We will explain a small lycaenid butterfly, *Callophrys rubi*, as an example. This butterfly is distributed widely in Eurasia and in North Africa and first

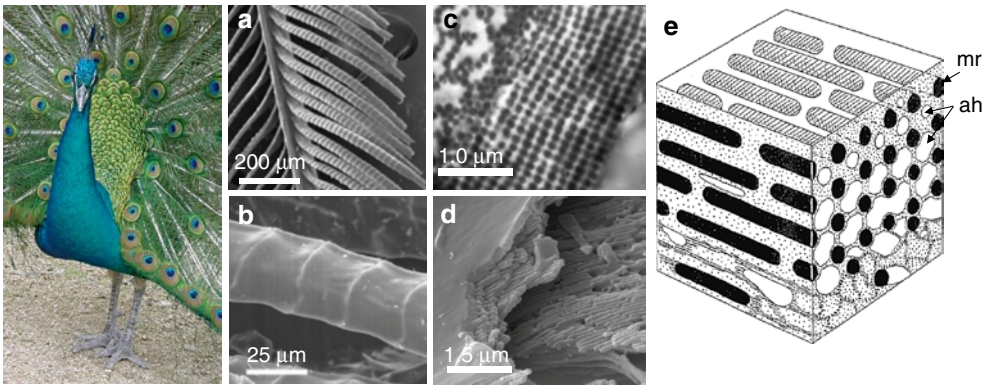

Fig. 10.12 Peacock, showing iridescent feathers. (**a**) part of feather barb, showing barbules, (**b**) segments of barbule, (**c**) cross section, and (**d**) fractured view of single barbule (Yoshioka and Kinoshita (2002); Kinoshita et al. 2008). (**e**) Schematic illustration of the internal architecture of the barbule with melanin rods (mr) and air holes (ah) (Reproduced from Durrer (1977), with permission)

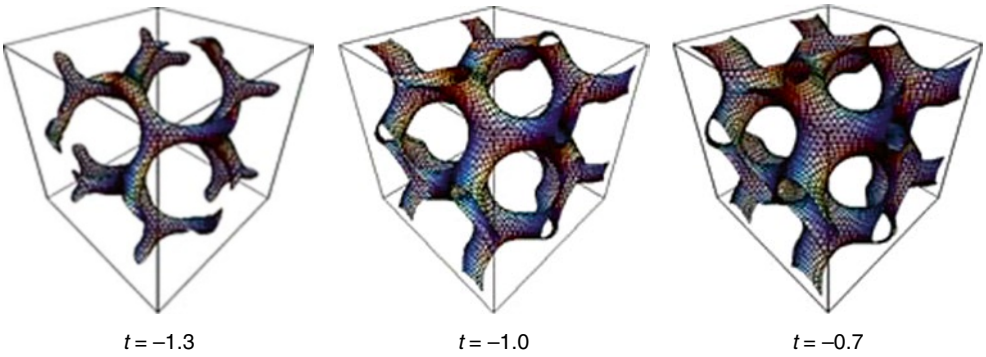

Fig. 10.13 Examples of gyroid structure for $t = -1.3$, -1.0, and -0.7

received attention by Onslow (1920, 1923). He noticed that a reflective scale of this butterfly showed irregular polygonal dark patches when observed under transillumination, hence the descriptor "mosaic scale" by Schmidt (1943). Afterward, the microstructure of this mosaic scale was investigated electron microscopically by Morris (1975). He observed that each polygonal grain, seen as a mosaic patch, was 5.4 μm in mean diameter and consisted of a simple cubic network with a lattice constant of 0.257 μm.

Ghiradella and Radigan (1976) also made an electron microscopic observation of the scale and observed a 3D photonic crystal that they interpreted as being cubic close packed, although it may in fact be a related form (see below). In any case, the elaborated structures in the interior of the *C. rubi* scales are now well known as typical examples of 3D biological photonic crystals, and the mosaic patches first observed within each scale about 100 years ago correspond to crystal domain structures having different lattice orientations.

Recently, it has been reported that these photonic structures can be expressed by a simple gyroid minimal surface, which is observed for block copolymer systems as a thermodynamically stable structure (Michielsen and Stavenga 2008; Saranathan et al. 2010). A gyroid is an infinitely connected 3D curved surface represented approximately by a mathematical expression

$$g(x, y, z) = t,$$

with

$$g(x, y, z) = \sin x \cos y + \sin y \cos z + \cos x \sin z,$$

which divides a 3D space into two according to a condition of $g(x, y, z) > t$ or $g(x, y, z) < t$ with t as a parameter. We show the examples of curved surface calculated for various t's in Fig. 10.13. If a space defined by $g(x, y, z) < t$ corresponds to a cuticle network, and that defined by $g(x, y, z) > t$ to a remaining air space, the photonic crystal structures found in the scales of various kinds of butterflies can be expressed fairly well by this formula. t in this case corresponds to a filling factor of cuticle network and it was reported that for *C. rubi*, t ranged $-1.4 < t < -1.0$, corresponding to the filling factor 0.16–0.26 (Michielsen and Stavenga 2008).

This proposal was experimentally confirmed by the comparison of calculated cross sections with TEM or SEM images (Michielsen and Stavenga 2008), by that of the reflection spectrum with the band calculation (Michielsen and Stavenga 2008; Poladian et al. 2009), by the finite-difference time-domain (FDTD) calculation (Michielsen et al. 2010), and also by the diffraction patterns obtained in small-angle X-ray scattering studies (Saranathan et al. 2010). Although these comparisons are not complete at the present

stage, they are expected to become clues to solving the problem of how these elaborate structures are formed during the pupal period of the butterflies.

10.5 Coloration Due to Random Structures

10.5.1 Rayleigh Scattering

The scattering of light does not in principle require regular structures to produce structural colors, and so it can be a most important source for colors with mechanisms completely different from those of thin-layer or photonic-crystal types. Light scattering is considered a light emission phenomenon due to an induced oscillating dipole under light illumination which emits light uniformly in different directions, so that it is basically non-iridescent; the color does not change with viewing angle. Thus, scattering has been thought of as a cause of bluish colors without directionality, which effect is generally found in a wide variety of random media. For example, the origin of the blue sky is explained as due to light scattering by atmospheric microparticles (Rayleigh 1871a, b), later called Rayleigh scattering. The pale bluish color of a suspension involving small colloidal particles is known as Tyndall blue. The blue or bluish color in these cases is based on the fact that scattering efficiency is proportional to the fourth power of light frequency and hence to an inverse of the fourth power of wavelength (inverse-fourth-power law).

Rayleigh scattering (see Chap. 1) is only applicable to a case where the particle size is sufficiently small as compared with the wavelength of light. When the particle size becomes larger, the deviation from the inverse-fourth-power law becomes remarkable and the light scattering in the visible region becomes enhanced. This is called Mie scattering, named after the research done by Mie (1908) on light scattering by metallic colloidal particles. With increasing particle size, the scattering direction largely changes from that of uniform Rayleigh scattering to that characterized by strong forward scattering (see Born and Wolf 1959).

In the past, Tyndall blue frequently appeared in the literatures as a typical example of a non-iridescent structural color. Mason (1923a, 1926) considered the colors of some birds and insects as due to Tyndall blue and used as examples the feather of a blue jay and the body/wing of a dragonfly. He proposed six necessary conditions for a medium to show the Tyndall blue: (1) inhomogeneities in the refractive index, (2) dimensions comparable to the wavelength of light, (3) blue scattering and red transmission, (4) size-dependent saturation of the blue color, (5) polarized scattering, and (6) inverse proportionality to the fourth power of wavelength.

Frank and Ruska (1939) applied the first commercially available electron microscope to investigate the feathers of the ivory-breasted pitta and the turquoise tanager, which were known to display Tyndall blue. Within barbs of the blue feathers, they found spongy structures consisting of keratin and air at the inner region of the medullary cell. Later, more detailed observation on the spongy structure was made by Schmidt and Ruska (1962) on several avian species. They reported that the spongy structure sometimes appeared to consist of numerous spherical or oval vacuoles, now called the *spherical type*, while at other times, they showed a network structure consisting of hard sticks and air holes, now called the *channel type* (Noh et al. 2010).

These spongy structures are now known to be widely distributed in avian species: kingfisher, parakeet, cotinga, jay, manakin, and bluebird are the well-known examples of this type. Until recently, however, it was generally believed that the Tyndall blue is the only cause for the blue colorations in these spongy structures. Yet, there were only a few reports to accurately measure the reflection spectrum, its angular dependence, and the polarization characteristics, which were the necessary conditions for Tyndall blue as proposed by Mason.

10.5.2 Coherent Scattering

However, it was gradually recognized that the light scattering was somehow modified and contributed effectively to animal colors. The first implication of the presence of interference phenomena on this problem was made by Raman (1934), who threw doubt on Tyndall scattering in the feather of an Indian roller. He found that the barb contained a series of cells whose colors varied from cell to cell. Further, he noticed that when the barb was fully damp, the dark blue changed into bright green and the light blue into light red. He compared these results with light scattering known for particles of various sizes and concluded light scattering does not suffice as explationation.

Dyck (1971) performed anatomical and optical investigations of the feathers of the rosy-faced love bird and plum-throated cotinga (*Cotinga maynana*). He found that the inner part of a barb was completely filled with a spongy structure, which consisted of a 3D network of connecting ca. 0.1-μm-wide keratin rods, which supported empty spaces ~0.1 μm in diameter. He investigated the spongy structures in various avian species and found that the widths of the rods and air spaces were strikingly uniform in size, while their orientations were definitely random. Furthermore, he found that the reflection spectrum showed a clear peak, which could not be explained in terms of the Rayleigh/Tyndall scattering (Fig. 10.14).

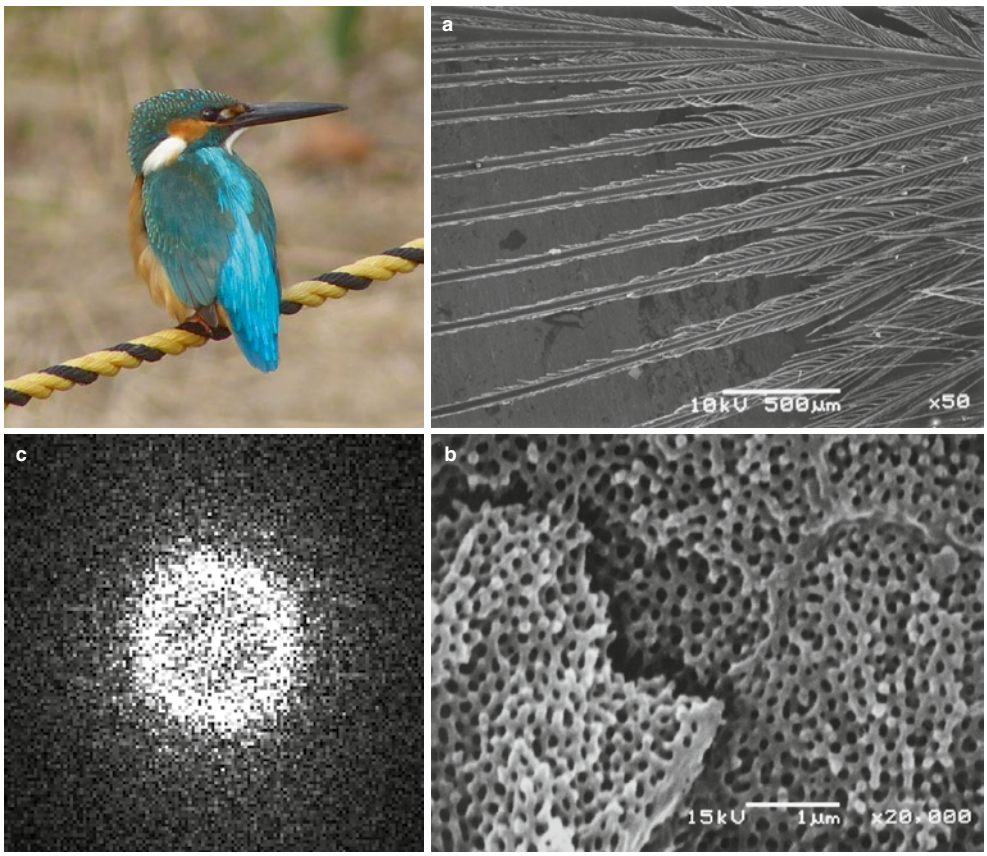

Fig. 10.14 (**a**) A common kingfisher, *Alcedo atthis*: (**a**) Barbs, (**b**) cross-section view of a fractured barb, (**c**) 2D Fourier image of the TEM image of its spongy structure (Reproduced from Kinoshita and Yoshioka 2005b)

Prum et al. (1998) played a decisive role in the solution of this problem. They employed a spatial Fourier transformation of a TEM image of the medullary spongy structure in the blue feather barbs of *C. maynana* and found a clear ring structure around the origin in wave vector space (see Fig. 10.14c for an example). If spongy structures with a wide variety of sizes are distributed, a Gaussian-like distribution would be obtained around the origin. The presence of a ring structure clearly indicates that a characteristic size of the network actually exists, which presumably corresponds to the reflection maximum.

Prum et al. (1998) simulated the reflection spectrum using the 2D Fourier power spectrum by averaging it radially and converting the radius of the ring into the peak position of the reflection spectrum, using the average refractive index. The result was in fairly good agreement with the experiment. They applied this method to the feathers of various other avian species (Prum et al. 1999a; Prum 2006) and to avian and mammalian skins (Prum et al. 1999b; Prum and Torres 2003, 2004), which appeared as quasi-ordered arrays of parallel collagen fibers, and found a similar spatial order.

Thus, it is now clear that the spongy structures generally possess a characteristic size which actually contributes to the generation of a well-defined reflection peak through constructive interference; Prum et al. (1998) called the light scattering of this type *coherent light scattering*. It also becomes clear that these structures are widely distributed in the animal kingdom, particularly in birds and insects. Their structural units appear sometimes in a form of a network and sometimes as randomly distributed spheres. These findings are quite important because the structure actually possesses short-range order, which induces the interference of light by enforcing reflection in a particular wavelength range.

Recently, Dufresne et al. (2009) employed small-angle X-ray scattering (SAXS) to analyze the spongy structures in various feather barbs and found similar ring structures both for channel and spherical types, as shown in Fig. 10.15. They found that the ring structure generally consisted of a definite ring, which was followed by a tail or a weak second ring outside the main ring (see Fig. 10.15c, d). Since the scattering efficiency of X-rays is very low, the structural information is directly obtainable without being disturbed by multiple scattering, which will thus be comparable with the Fourier analysis performed by Prum et al. (1998).

Further, Noh et al. (2010) measured the reflection spectra under various optical configurations and found that under directional lighting, the feather barbs were surprisingly iridescent, while under omni-directional illumination, they were actually non-iridescent: the reflection spectrum was evidently independent of the angle of incidence, if the refraction at the

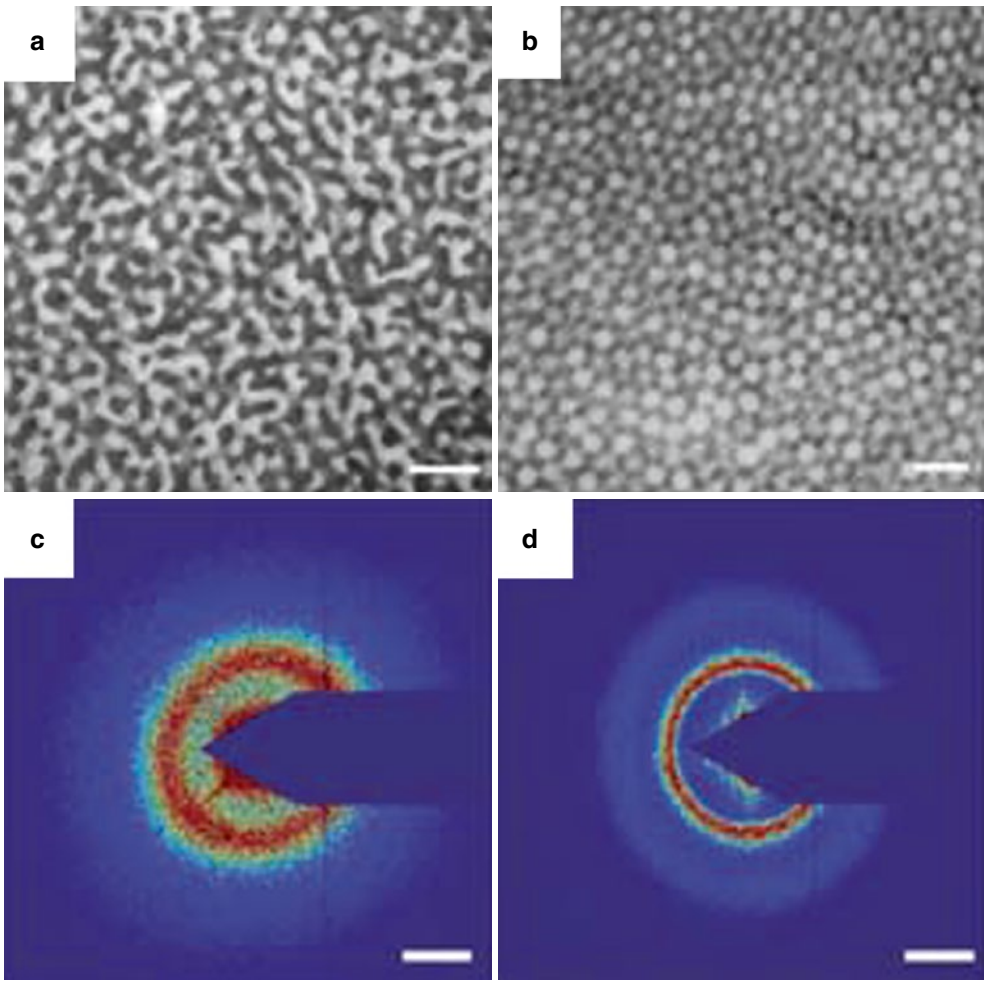

Fig. 10.15 Electron micrographs of feather barbs of (**a**) channel-type male eastern bluebird (*Sialia sialis*) and (**b**) sphere-type male plum-throated cotinga (*Cotinga maynana*), and the corresponding small-angle X-ray scattering patterns, (**c**) and (**d**). Scale bars are 500 nm for (**a**) and (**b**), and 0.025 cm^{-1} for (**c**) and (**d**) (Reproduced from Dufresne et al. (2009), with permission)

surface was properly corrected, and was dependent only on an angle between the directions of incidence and reflection. The authors attempted to reproduce the reflection spectrum from the SAXS pattern and obtained good agreement with respect to the main ring when the average refractive index was set at 1.25.

From the standpoint of spectral tuning, the spongy structure gives rather weak tuning capability, because its coloring mechanism is essentially based on random structure that is slightly modified by the presence of short-range order. However, it offers a special effect as compared to the ordinary interference-type structural color: the important point is that it is basically non-iridescent, so it does not show directionality, which eventually prevents the lustrous appearance. On the other hand, this rather passive mechanism results in the degradation of the reflection efficiency, which is, however, compensated for by placing dark pigments below the spongy structure. Thus, the interplay of pigmentary and structural colors is essential in this system, as it is in others, for example, the deep blue thin-film reflective scales of many of the *Morpho* butterflies (see below).

10.6 Diversity of Structural Colors

10.6.1 Morpho Butterflies

Very complicated structures, in which both multilayer interference and grating effects contribute to colors, have been often observed in nature, especially in the scales of butterfly wings (Ghiradella 1994, 1998). The most remarkable example is the *Morpho* butterfly inhabiting the New World from Central to South America. The wings of this butterfly display striking, even metallic, blue and have been attracting scientists' interest from the nineteenth century. Their surprisingly elaborate microstructures became clear just after the invention of electron microscope (Anderson and Richards 1942, Gentil 1942). The most remarkable features in the optical response of their wings are that while they strongly reflect the blue light, the reflection direction spreads widely but only within a plane nearly perpendicular to the ridge direction on the scale (the ridges are longitudinal folds projecting from the obverse surface of most butterfly scales) (Vukusic

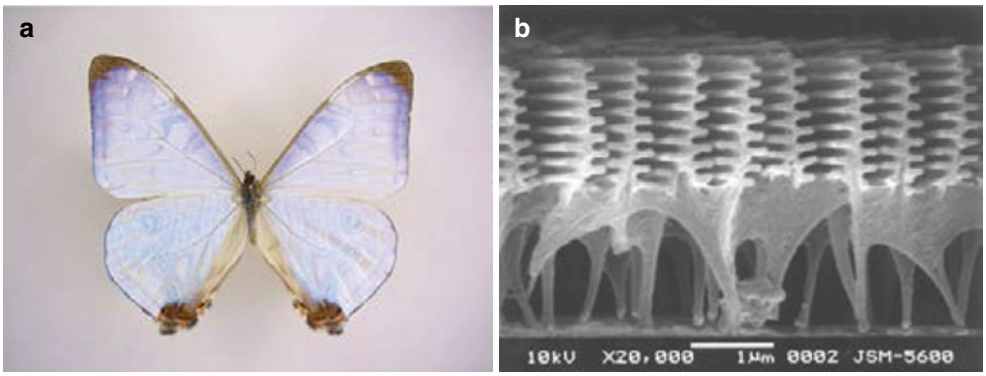

Fig. 10.16 (**a**) *Morpho sulkowskyi* and (**b**) scanning electron microscopic image of a cross section of a reflective scale

et al. 1999, Kinoshita et al. 2002a, b). Various models have been proposed so far and numerical calculations of diverse kinds have been performed to elucidate the mechanism of this blue reflection (Gralak et al. 2001; Kinoshita et al. 2002b; Plattner 2004; Zhu et al. 2009; Lee and Smith 2009).

It is now generally understood that the strongly blue and widely spreading reflections are caused by a unique scale ridge structure. As shown in Fig. 10.16b, the ridges are densely distributed at intervals of ~1 μm on a scale; they extend longitudinally for almost the full length of the scale. Each ridge has stacks of thin shelves, or *lamellae*, which project alternately from each side as shown in Fig. 10.16b; these and the air spaces between them form the mirror. This unique structure causes the miraculous balance of a multilayer interference and diffraction effect that is restricted to a plane perpendicular to the ridge direction (Kinoshita et al. 2002a, Kinoshita 2013). Further, the alternately configured lamellae can be regarded as obliquely inclining lamellae and enhance the backscattering when illuminated from oblique directions. This will make the blue wing more vivid without being disturbed by the specular reflection (Kambe et al. 2011). The color of the wing is largely affected by underlying melanin layers, which absorb the light other than blue, thereby ensuring the deep blue color. Lacking such underlying pigment, the scales are translucent and "pearlescent," with only a pale blue color (see Fig. 10.16a). Thus, plenty of architectural designs in addition to cooperation with pigment bestow such a beautiful color on this butterfly and on other reflective creatures.

10.6.2 Liquid Crystals

There exists in nature yet another class of structural color mechanism. Chemists have long known that certain liquid crystal molecules orient themselves in certain very specific fashions. One such is the so-called "helicoidal," "cholesteric," or "chiral" arrangement: the molecules are arrayed such that their orientation *precesses*, being in each layer slightly rotated with respect to those in the layer below. The thickness of the layers and the direction ("chirality") of the rotation can be tunable, and if tuned properly, they will produce structural colors that are analogous to multilayer stack colors.

Many thermometers using this type of liquid crystal are on the market; these work by reversibly changing their colors when the temperature is increased or decreased (thereby changing the thickness of the "layers" and hence the optical properties). A similar phenomenon occurs in biological systems; if collagen, chitin, or other biological fibrils are arranged in a regular helicoid fashion, the system can be tuned to produce color; this is the basis for the iridescent cuticles of many beetles, flies, and other insects (for reviews, see Neville 1993 and Srinivasarao 1999; see Lee 2007 for a discussion of this mechanism in plant coloration). The light reflected from these helicoid arrays is circularly polarized; the chirality of biological systems has seemed uniformly to reflect left-circularly polarized light, but at least one beetle has found a way to simultaneously reflect both left and right circularly polarized lights (Caveney 1971).

10.6.3 Interplay with Pigments

Let us bring the pigments back into play by noting that many organisms combine structural and pigmentary colors to get additional special effects. In birds, green plumage is often achieved by combining a structural blue color with a pigment yellow. As described above, in many, but not all, blue *Morpho* butterflies, a pigmentary "backing" intensifies the structural blue color by absorbing unwanted light entering the reflecting structures, because the wavelengths of such light are located in a range other than blue, are also likely to be out of phase with the "functional" light, and would dilute the purity of the interference color. In a species of *Morpho* butterflies, white spots on the wing are produced simply by removing the backing pigments in these areas, while the elaborate

microstructures are left untouched (Yoshioka and Kinoshita 2006). Since, after passing the reflecting structure, light of wavelengths other than blue is scattered by the underlying wing membrane and scales on the reverse side, it comes back to the obverse side without directionality and is perceived by the viewers as white spots on the wing.

10.6.4 Whiteness and Transparency

The biological world has a few additional ways of handling light. Scattering produces brilliant whites (Vukusic et al. 2007) and may yield more complex effects, especially if the combined optical behavior of all scales in a wing transect is taken into account (Stavenga et al. 2006b) or if structures and pigments interact to produce "emergent" optical effects (Rutkowski et al. 2005; Morehouse et al. 2007). And of course there is transparency, a highly effective technique for evading predators. We have already mentioned antireflective coatings, in particular the nipples that allow clearwing moths to become essentially invisible against any background (Yoshida et al. 1996; Yoshida 2002). But invisibility is best understood in the open seas (see Herring 2002, Wilson and Hastings 2013 for review), where there is no place to hide. Coelenterates and ctenophores may build bodies largely of transparent jelly, but arthropods and vertebrates must have muscles and skeletons. To some degree, these can be rendered transparent by arranging fibrous proteins so that they produce destructive interference in the predominantly blue light in their environment(s). But eyes must have pigment and gut contents quickly become opaque, even if they do not start that way. This may be the reason why so many fishes have instead evolved silvery mirrored sides to render themselves invisible.

10.6.5 Relation to Fluorescence

No discussion of spectral tuning would be complete without a brief mention of fluorescence, the process by which light of a relatively short wavelength is absorbed and reemitted at a longer wavelength (see Chap. 1). This has been reported to be widespread in spiders (Andrews et al. 2007), where it may have communication and possibly metabolic and other functions as well.

A particularly intriguing case is described in a *Papilio* butterfly (Vukusic and Hooper 2005); the reflective scales have 2D photonic crystals on their obverse surfaces; these collimate the light so that it is effectively emitted upward (or reflected with a help of a mirror lining the reverse surface) for the wavelengths of light at around 505 nm. This wavelength just matches a peak of a fluorescent pigment fused in the 2D photonic crystals as also does the central range of the animal's green visual pigment. Thus, the 2D photonic crystal in this case may be placed to successfully extract fluorescent light from the wing. A similar mechanism is now often used in light-emitting diodes to extract the light efficiently from the device, another example of biomimicry.

10.6.6 Biomimicry

In closing, we would like to revisit briefly some of the ideas and systems that we have discussed and present some additional information. First is biomimicry. We have alluded to the burgeoning interest in the field, even reaching into architectural design (Aldersey-Williams 2004). There has been particular interest in duplicating the *Morpho* iridescent scale system (e.g., Aryal et al. 2012), but other systems are being studied widely. Two books written for popular audiences are Benyus (2002) and Harman (2013); the latter considers some of the general economic and business concomitants of some of the systems.

In a related vein, scientists have realized that the highly structured *Morpho* wing might provide the design for a chemical sensor: gas molecules penetrating between the lamellae will change the refractive index of the air component and hence the reflectivity of the scale (Potyrailo et al. 2007). There is little question that more of these biological structures will have much to teach us about design.

10.6.7 Developmental Studies on Microstructures

One particularly intriguing question (actually allied to that of biomimicry) is how the organisms make these structures and materials in the first place. For many of those discussed above, the question remains to be investigated, but Ghiradella (1974, 1989) studied the development of the multilayer lamellae in the butterfly *Colias eurytheme* and of the 3D photonic crystals in another butterfly *Mitoura grynea*.

In the first case, it was possible to conjecture from the internal geometry (including the placement of actin bundles of the developing scale) that longitudinal tensile stress on the scale obverse epicuticular layer (the outer "envelope" of the nascent cuticle) may result in so-called elastic buckling, a common physical process that typically gives rise to regular and even folds. This has not been confirmed, but given the generality of regular folds in nonliving biological structures, it is almost certain that a common mechanism underlies this particular geometry.

The basis of the pattern formation is clearer with regard to the 3D photonic crystals; the smooth endoplasmic reticulum organizes itself into a 3D lattice; the cell then pulls in and weaves through the lattice space tubes of cell membrane

within which the cuticle is secreted, as cuticle always is, extracellularly. A variation of same system is obtained in striated muscle, in which the sarcoplasmic reticulum (the muscle cell's smooth endoplasmatic reticulum) organizes itself in such a way that the T-tubule invaginations of the cell membrane can carry the excitation from the nerve end plate deep into the contractile machinery.

References

Aldersley-Williams H (2004) Towards biomimetic architecture. Nat Mater 3:277–279

Anderson TF, Richards AG Jr (1942) An electron microscope study of some structural colors of insects. J Appl Phys 13:748–758

Andrews K, Reed SM, Masta SE (2007) Spiders fluoresce variably across many taxa. Biol Lett 3:265–267

Aryal M, Ko DH, Tumbleston JR, Gadisa A, Samulski ET, Lopez R (2012) Large area nanofabrication of butterfly wing's three dimensional ultrastructures. J Vac Sci Technol B 30:06182-1–06182-7

Benyus JM (2002) Biomimicry: innovation inspired by nature. Harper Collins, New York

Bernhard CG, Miller WH, Møller AR (1965) The insect corneal ripple array. A biological broad-band impedance transformer acts as an antireflection coating. Acta Physiol Scand 63(suppl 243):1–79

Bernhard CG, Gemne G, Møller AR (1968) Modification of specular reflexion and light transmission by biological surface structure – to see, to be seen or not to be seen. Quart Rev Biophys 1:89–105

Bernhard CG, Gemne G, Sällström J (1970) Comparative ultrastructure of corneal surface topography in insects with aspects on phylogenesis and function. Z Vergl Physiol 67:1–25

Berthier S (2007) Iridescences: the physical colors of insects. Springer, Berlin

Born M, Wolf E (1959) Principles of optics. Pergamon Press, London

Caveney S (1971) Cuticle reflectivity and optical activity in scarab beetles: the rôle of uric acid. Proc R Soc Lond B 178:205–225

DeMartini DG, Krogstad DV, Morse D (2013) Membrane invaginations facilitate reversible water flux driving tunable iridescence in a dynamic biophotonic system. Proc Natl Acad Sci U S A 110:2552–2556

Denton EJ, Land MF (1971) Mechanism of reflection in silvery layers of fish and cephalopods. Proc Roy Soc Lond A 178:43–61

Dufresne ER, Noh H, Saranathan V, Mochrie SGJ, Cao H, Prum RO (2009) Self-assembly of amorphous biophotonic nanostructures by phase separation. Soft Matter 5:1792–1795

Durrer H (1962) Schillerfarben beim Pfau (*Pavo cristatus* L.). Verhand Naturf Ges Basel 73:204–224

Durrer H (1977) Schillerfarben der Vogelfeder als Evolutionsproblem. Denkschr Schweiz Naturforsch Ges 91:1–127

Dyck J (1971) Structure and colour-production of the blue barbs of *Agapornis roseicollis* and *Cotinga maynana*. Z Zellforsch 115:17–29

Fox DL (1976) Animal biochromes and structural colours. University California Press, Berkeley

Frank F, Ruska H (1939) Übermikroskopische Untersuchung der Blaustruktur der Vogelfeder. Nature 27:229–230

Gentil K (1942) Elektronenmikroskopische Untersuchung des Feinbauses schillernder Leisten von Morpho-Schuppen. Z Morph Ökol Tiere 38:344–355

Ghiradella H (1974) Development of ultra-reflective butterfly scales: How to make an interference filter. J Morph 142:395–410

Ghiradella H (1984a) Development of ultraviolet reflecting butterfly scales: how to make an interference filter. J Morph 142:395–410

Ghiradella H (1984b) Structure of iridescent lepidopteran scales: variations on several themes. Ann Entomol Soc Am 77:637–645

Ghiradella H (1985) Structure and development of iridescent lepidopteran scales: the Papilionidae as a showcase family. Ann Entomol Soc Am 78:252–264

Ghiradella H (1989) Structure and development of iridescent butterfly scales: lattices and laminae. J Morph 202:69–88

Ghiradella H (1991) Light and color on the wing: structural colors in butterflies and moths. Appl Opt 30:3492–3500

Ghiradella H (1994) Structure of butterfly scales: patterning in an insect cuticle. Micr Res Tech 27:429–438

Ghiradella H (1998) Hairs, bristles and scales. In: Harrison FW, Locke M (eds) Microscopic anatomy of invertebrates, vol 11A, Insecta. Wiley-Liss, New York, pp 257–287

Ghiradella H, Radigan W (1976) Development of butterfly scales II. Struts, lattices and surface tension. J Morph 150:279–298

Glover BJ, Whitney HM (2010) Structural colour and iridescence in plants: the poorly studied relations of pigment colour. Ann Bot 105:505–511

Gralak B, Tayeb G, Enoch S (2001) Morpho butterfly wings color modeled with lamellar grating theory. Opt Exp 9:567–578

Hariyama T, Hironaka M, Horiguchi H, Stavenga DG (2005) The leaf beetle, the jewel beetle, and the damselfly: insects with a multilayered show case. In: Kinoshita S, Yoshioka S (eds) Structural colors in biological systems: principles and applications. Osaka University Press, Osaka, pp 153–176

Harman J (2013) The Shark's paintbrush. White Cloud Press, Ashland

Herring (1994) Reflective systems in aquatic animals. Comp Biochem Physiol 109A:513–546

Herring P (2002) The biology of the deep ocean. Oxford University Press, Oxford

Hinton HE, Jarman GM (1972) Physiological color change in the Hercules beetle. Nature 238:160–161

Hinton HE, Jarman GM (1973) Physiological color change in the elytra of the Hercules beetle. Dynastes hercules J Insect Physiol 19:533–549

Hooke R (1665) Micrographia: or same physiological descriptions of minute bodies made by magnifying glasses with observations and inquiries thereupon. Replicated by Dover Publication, New York

Huxley AF (1968) A theoretical treatment of the reflexion of light by multilayer structures. J Exp Biol 48:227–245

Kambe M, Zhu D, Kinoshita S (2011) Origin of retroreflection from a wing of the Morpho butterfly. J Phys Soc Jpn 80:054801-1–054801-10

Kinoshita S (2008) Structural colors in the realm of nature. World Scientific Publishing, Singapore

Kinoshita S (2013) Nanobiophotonics – an introductory textbook. Pan Stanford, Singapore

Kinoshita S, Yoshioka S (eds) (2005a) Structural colors in biological systems. Osaka University Press, Osaka

Kinoshita S, Yoshioka S (2005b) Structural colors in nature. A role of regularity and irregularity in the structure. ChemPhysChem 6:1443–1459

Kinoshita S, Yoshioka S, Kawagoe K (2002a) Mechanisms of structural color in the *Morpho* butterfly: cooperation of regularity and irregularity in an iridescent scale. Proc R Soc Lond B269:1417–1422

Kinoshita S, Yoshioka S, Fujii Y, Okamoto N (2002b) Photophysics of structural color in the *Morpho* butterflies. Forma 17:103–121

Kinoshita S, Yoshioka S, Miyazaki J (2008) Physics of structural colors. Rep Prog Phys 71:076401-1–076401-30

Land MF (1966) A multilayer interference reflector in the eye of the scallop, Pecten maximus. J Exp Biol 45:433–447

Land MF (1972) The physics and biology animal reflectors. Prog Biophys Mol Biol 24:77–106

Land MF, Nilsson D-E (2008) Animal eyes, 2nd ed. Oxford University Press, Oxford

Large MCJ, McKenzie DR, Parker AR, Steel BC, Ho K, Bosi SG, Nicorovici N, McPhedran RC (2001) The mechanism of light reflectance in silverfish. Proc R Soc Lond A 457:511–518

Lee D (2007) Nature's Palette: the science of plant color. University of Chicago Press, Chicago

Lee RT, Smith GS (2009) Detailed electromagnetic simulation for the structural color of butterfly wings. Appl Opt 48:4177–4190
Lythgoe JN, Shand J (1982) Changes in spectral reflexions from the iridophores of the neon tetra. J Physiol 325:23–34
Mason CW (1923a) Structural colors in feathers. I. J Phys Chem 27: 201–251
Mason CW (1923b) Structural colors in feathers. II. J Phys Chem 27:401–447
Mason CW (1926) Structural colors in insects. I. J Phys Chem 30:383–395
Mason CW (1927a) Structural colors in insects. II. J Phys Chem 31: 321–354
Mason CW (1927b) Structural colors in insects. III. J Phys Chem 31: 1856–1872
Michielsen K, Stavenga DG (2008) Gyroid cuticular structures in butterfly wing scales: biological photonic crystals. J R Soc Interface 5:85–94
Michielsen K, De Raedt H, Stavenga DG (2010) Reflectivity of the gyroid biophotonic crystals in the ventral wing scales of the green hairstreak butterfly. Callophyris rubi J R Soc Interface 7:765–771
Mie G (1908) Beiträge zur Optik trüber Meien, speziell kolloidaler Metallösungen. Annu Rev Plant Physiol Plant Mol Biol 330: 377–445
Morehouse NI, Vukusic P, Rutkowski R (2007) Pterin pigment granules are responsible for both broadband light scattering and wavelength selective absorption in the wing scales of pierid butterflies. Proc Roy Soc Lond B 274:359–366
Morris RB (1975) Iridescence from diffraction structures in the wing scales of *Callophrys rubi*, the Green Hairstreak. Proc R Soc Entomol A 48:149–154
Nagaishi H, Oshima N (1992) Ultrastructure of the motile iridophores of the neon tetra. Zool Sci 9:65–75
Neville AC (1993) Biology of fibrous composites. Cambridge University Press, Cambridge
Newton I (1704) Opticks: or a treatise of the reflections, refractions, inflections & colours of light. Republicated by Dover Publication, New York
Noh H, Liew SF, Saranathan V, Mochrie SGJ, Prum RO, Dufresne ER, Cao H (2010) How noniridescent colors are generated by quasi-ordered structures of bird feather. Adv Mater 22:2871–2880
Onslow H (1920) The iridescent colours of insects. II. Diffraction colours. Nature 106:181–183
Onslow H (1923) On a periodic structure in many insect scales, and the cause of their iridescent colours. Phil Trans 211:1–74
Parker AR (1998) The diversity and implications of animal structural colours. J Exp Biol 201:2343–2347
Parker AR (1999) Light-reflection strategies. Am Sci 87:248–255
Parker AR (2000) 515 million years of structural color. J Opt A Pure Appl Opt 2:R15–R28
Parker AR, McPhedran RC, McKenzie DR, Botten LC, Nicorovici N-AP (2001) Aphrodite's iridescence. Nature 409:36–37
Parker AR, Welch VL, Driver D, Martini N (2003) An opal analogue discovered in a weevil. Nature 426:786–787
Pfaff G, Reynders P (1999) Angle-dependent optical effects from submicron structures of films and pigments. Chem Rev 99:1963–1981
Plattner L (2004) Optical properties of the scales of *Morpho rhetenor* butterflies: theoretical and experimental investigation of the back-scattering of light in the visible spectrum. J R Soc Interface 1:49–59
Poladian L, Wichham S, Lee K, Large MCJ (2009) Iridescence from photonic crystals and its suppression in butterfly scales. J R Soc Interface 6:S233–S242
Potyrailo RA, Ghiradella H, Vertiatchikh A, Dovidenko K, Cournoyer JR, Olson E (2007) *Morpho* butterfly wing scales demonstrate highly selective vapour response. Nat Photonics 1:123–128
Prum RO (2006) Anatomy, physics and evolution of structural colors. In: Hill GE, McGraw KJ (eds) Bird coloration, vol 1, Mechanisms and measurements. Harvard University Press, Cambridge, MA, pp 295–353
Prum RO, Torres RH (2003) Structural colouration of avian skin: convergent evolution of coherently scattering dermal collagen arrays. J Exp Biol 206:2409–2429
Prum RO, Torres RH (2004) Structural colouration of mammalian skin: convergent evolution of coherently scattering dermal collagen arrays. J Exp Biol 207:2157–2172
Prum RO, Torres RH, Williamson S, Dyck J (1998) Coherent light scattering by blue feather barbs. Nature 396:28–29
Prum RO, Torres RH, Williamson S, Dick J (1999a) Two-dimensional fourier analysis of the spongy medullary keratin of structurally coloured feather barbs. Proc R Soc Lond B266:13–22
Prum RO, Torres RH, Kovach F, Williamson S, Goodman SM (1999b) Coherent light scattering by nanostructured collagen arrays in the caruncles of the *Malagasy asities* (Eurylaimidae: Aves). J Exp Biol 202:3507–3522
Raman CV (1934) The origin of the colours in the plumage of birds. Proc Ind Acad Sci A1:567–573
Rayleigh JWS (1871a) On the light from the sky, its polarization and colour. Phil Mag 41:107–120
Rayleigh JWS (1871b) On the scattering of light by small particles. Phil Mag 41:447–454
Rutkowski RL, Macedonia JM, Morehouse N, Taylor-Taft L (2005) Pterin pigments amplify iridescent ultraviolet signal in males of the orange sulphur butterfly, Colias eurytheme. Proc R Soc Lond B 272:2329–2335
Saranathan V, Osuji CO, Mochrie SGJ, Noh H, Narayanan S, Sandy A, Dufresne ER, Prum RO (2010) Structure, function, and self-assembly of single network gyroid (14_i32) photonic crystals in butterfly wing scales. Proc Natl Acad Sci 107:11676–11681
Schmidt WJ (1943) Die Mosaikschuppen des *Teinopalpus imperialis* Hope, ein neues Muster schillernder Schmetterlingsschuppen. Z Morph Ökol Tiere 39:176–216
Schmidt WJ, Ruska H (1962) Tyndallblau – Structur von Federn im Elektronenmikroskop. Z Zellforsch 56:693–708
Srinivasarao M (1999) Nano-optics in the biological world: beetles, butterflies, birds, and moths. Chem Rev 99:1935–1961
Stavenga DG, Foletti S, Palasantzas G, Arikawa K (2006a) Light on the moth-eye corneal nipple array of butterflies. Proc R Soc Lond B 273:661–667
Stavenga DG, Giraldo MA, Hoenders BJ (2006b) Reflectance and transmittance of light scattering scales stacked on the wings of pierid butterflies. Opt Exp 14:4880–4890
Vigneron JP, Pasteels JM, Windsor DM, Vértesy S, Rassart M, Seldrum T, Dumont J, Deparis O, Lousse V, Biró L, Ertz D, Welch V (2007) Switchable reflector in the Panamanian tortoise beetle, Charidotella egregia (Chrysomelidae: Cassinidae). Phys Rev E 76:031907-1–031907-10
Vukusic P, Hooper I (2005) Directionally controlled fluorescence emission in butterflies. Science 310:1151
Vukusic P, Sambles JR (2003) Photonic structures in biology. Nature 424:852–855
Vukusic P, Sambles JR, Lawrence CR, Wootton RJ (1999) Quantified interference and diffraction in single *Morpho* butterfly scales. Proc R Soc Lond B 266:1403–1411
Vukusic P, Hallam B, Noyes J (2007) Brilliant whiteness in ultrathin beetle scales. Science 315:348
Welch VL, Vigneron JP, Parker AR (2005) The cause of colouration in the ctenophore, *Beroë cucumis*. Curr Biol 15:R985–R986
Wilson T, Hastings JW (2013) Bioluminescence: living lights, lights for living. Harvard University Press, Cambridge, MA
Yoshida A (2002) Antireflection of butterfly and moth wings through microstructure. Forma 17:75–89

Yoshida A, Motoyama M, Kosaku A, Miyamoto K (1996) Nanoprotuberance array in the transparent wing of a hawkmoth, *Cephonodes Hylas*. Zool Sci 13:525–526

Yoshioka S, Kinoshita S (2002) Effect of macroscopic structure in iridescent color of the peacock feathers. Forma 17:169–181

Yoshioka S, Kinoshita S (2006) Structural or pigmentary? Origin of the distinctive white stripe on the blue wing of a Morpho butterfly. Proc R Soc Lond B273:129–134

Yoshioka S, Kinoshita S (2011) Direct determination of the refractive index of natural multilayer systems. Phys Rev E 83:051917-1–051917-7

Yoshioka S, Nakamura E, Kinoshita S (2007) Origin of two-color iridescence in rock dove's feather. J Phys Soc Jpn 76: 013801-1–013801-4

Yoshioka S, Matsuhana B, Tanaka S, Inouye Y, Oshima N, Kinoshita S (2011) Mechanism of variable structural colour in the neon tetra: quantitative evaluation of the Venetian blind model. J R Soc Interface 8:56–66

Zhu D, Kinoshita S, Cai D, Cole JB (2009) Investigation of structural colors in Morpho butterflies using the nonstandard-finite-difference time-domain method: Effects of alternately stacked shelves and ridge density. Phys Rev E 80:051924-1–051924-12

Zi J, Yu X, Li Y, Hu X, Xu C, Wang X, Liu X, Fu R (2003) Coloration strategies in peacock feathers. Proc Natl Acad Sci 100: 12576–12578